Available online at www.sciencedirect.com
ScienceDirect
Scripta Materialia 61 (2009) 863–866
Scripta MATERIALIA
www.elsevier.com/locate/scriptamat

Strains and strain rates during friction stir welding

A. Arora,[a] Z. Zhang,[a] A. De[b] and T. DebRoy[a,*]

[a] *Department of Materials Science and Engineering, The Pennsylvania State University, 115 Steidle Building, PA 16802, USA*
[b] *Department of Mechanical Engineering, IIT Bombay, Bombay, India*

Received 29 May 2009; revised 16 July 2009; accepted 17 July 2009
Available online 21 July 2009

Strains experienced by materials during friction stir welding (FSW) are important but scarce in the literature. Here we report the computed strains and strain rates during FSW of AA2524 from a three-dimensional coupled viscoplastic flow and heat transfer model. The strain rates are integrated along a streamline to estimate the accumulated strains experienced by the material. The computed strains and strain rates were in the ranges −10 to 5 and −9 to 9 s^{-1}, respectively.

Keywords: Friction stir welding; Aluminum alloy; Modelling; Convection; High temperature deformation

Local gradients of temperature, strain rate and strains in the stir zone (SZ) and thermomechanically affected zone (TMAZ) influence the microstructure and mechanical properties of the friction stir welded parts [1]. In large-deformation processes the accumulated strain is an important factor affecting the nucleation and dynamic recrystallization rates, and ultimately the final grain structure [2–7]. The local strain values affect the critical nuclei diameter, the nucleation rate and the extent of formation of lo- angle grain boundaries in the stir zone [3,6].

Equivalent strains in friction stir welding (FSW) were computed by Buffa et al. [8,9] and Schimdt and Hattel [10] using solid mechanics. The maximum values of equivalent strain varied from 6 [8,9] to 133 [10] for different welding conditions. Bastier et al. [11] also reported the computed values of total strain components in FSW based on a solid mechanics model with precalculated temperature fields obtained from a separate heat generation and computational fluid dynamics (CFD)-based heat transfer model of the stir zone. The computed normal strain (ε_{33}) was tensile in nature, while the transverse strain (ε_{22}) was compressive. The longitudinal strain (ε_{11}) was significantly smaller than the other two components. However, the values of the strain components were significantly smaller than the values of effective strain reported earlier [8–10]. In view of the scarcity of the strain values and the wide range of the reported values, there is a need to expand the values of the effective or equivalent strain and the strain components in the SZ and TMAZ during FSW.

Direct measurements of the strain in the SZ and TMAZ are difficult due to the movement of materials around the tool during FSW [1]. One solution is to compute the values of the strain distributions in the SZ and TMAZ from a FSW model. Viscoplastic material flow and heat transfer based numerical models have been developed in recent years to understand the heat generation rate, temperature fields, materials flow and strain rates during FSW [12–17]. These numerical models have been validated by comparing the computed results with the corresponding experimentally measured temperature profiles and the size of the TMAZ. So far, these models have not been used to predict the strain values. Here we show a method to calculate the strain components using a three-dimensional viscoplastic flow and heat transfer model, and to validate the methodology using independent experimental data; we discuss the computed strains for typical FSW of AA2524 alloy.

The three-dimensional viscoplastic flow and heat transfer model used in the present work has been reported elsewhere [15–17] and therefore is not repeated here. The numerical model computes the velocity and the temperature field. Strain hardening has been ignored while computing velocity and temperature field. The strain rate is computed from the local velocity gradients:

$$\dot{\varepsilon}_{ij} = \frac{1}{2}\left(\frac{\partial u_i}{\partial x_j} + \frac{\partial u_j}{\partial x_i}\right), \tag{1}$$

* Corresponding author. Tel.: +1 814 865 1974; e-mail: debroy@psu.edu

1359-6462/$ - see front matter © 2009 Acta Materialia Inc. Published by Elsevier Ltd. All rights reserved.
doi:10.1016/j.scriptamat.2009.07.015

where $\dot{\varepsilon}_{ij}$ is the strain rate tensor and $\frac{\partial u_i}{\partial x_j}$ is the velocity gradient. The strain is computed next by integrating the strain rate tensor with time along a streamline [18]:

$$\varepsilon_{ij} = \int_0^t \dot{\varepsilon}_{ij}\, dt, \tag{2}$$

where ε_{ij} is the strain tensor, and dt is the time step for integration. Since a streamline represents the path a particle is expected to follow in the flow field, the local strain computed by Eq. (2) will depict the total strain experienced by the particle at a spatial location.

Since the viscoplastic flow and heat transfer calculations are done considering a steady-state flow, time is not a variable in the calculations. To obtain the time variable, the streamlines are divided into 60 points. For two closely placed points on the streamline, the ratio of the local velocity and the distance between the points will give the time taken by a particle to travel between the two points as:

$$dt = \frac{\Delta x_s}{u_s}, \tag{3}$$

where Δx_s is the distance between two points on the streamline and u_s is the resultant velocity along the streamline between the two points. From Eqs. (1)–(3), for n (=60) points on a streamline, the strain tensor can now be computed as follows:

$$\varepsilon_{ij} = \sum_{k=1}^{n-1} \frac{1}{2}\left(\frac{\partial u_i}{\partial x_j} + \frac{\partial u_j}{\partial x_i}\right)^k \times \left(\frac{\Delta x_s}{u_s}\right)^k, \tag{4}$$

where k is the number of points along the streamline, Δx_s is the distance between point k and $k+1$, and u_s is the velocity at point on the streamline. FSW of AA2524 is considered for all the calculations.

The method to compute the strain rates and strains along a streamline is verified by comparing the computed strains with the corresponding experimentally determined strains in an extrusion experiment reported by Berghaus et al. [18]. They determined strain values from changes in the flow line shapes during axisymmetric extrusion of aluminum billets at 430 °C with an extrusion ratio of 12.4:1 using an ink-grid method. Figure 1 shows that the computed values on the extruded surface from the streamline integration method are in good agreement with the independent experimentally determined values. The agreement shows that the methodology can be used to compute the strain values in a high-strain process such as FSW.

A viscoplastic flow and heat transfer model has been used to predict the temperature and material flow fields during FSW of aluminum alloy AA2524 in three dimensions using the material properties and experimental conditions reported in the literature [17]. The welding velocity is 2.11 mm s^{-1} and tool rotational velocity is 300 rpm. Figure 2 shows the computed velocity fields in horizontal planes 0.133 and 2.0 mm below the work piece surface during FSW. The welding direction and the direction of tool rotation are also shown in the figure. The five streamlines in Figure 2 are drawn using the computed velocity field. The region between streamlines 1 and 5 contains the SZ, TMAZ and the region through which the material flows. The x-axis indicates the distance along the welding direction with the tool located at $x = 0$. Similarly, the y-axis represents the

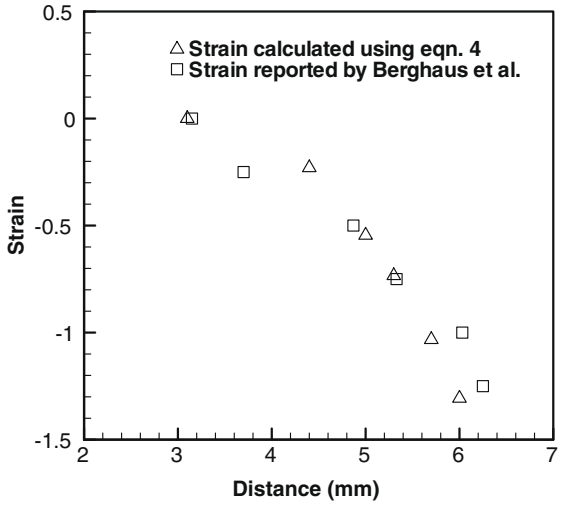

Figure 1. The strain values computed for the extrusion of an aluminum billet to verify the formulation of streamline integration method. The values shown by the squares are from the experimental results of Berghaus et al. [14] and the values shown by the triangles are from the methodology adapted in this work.

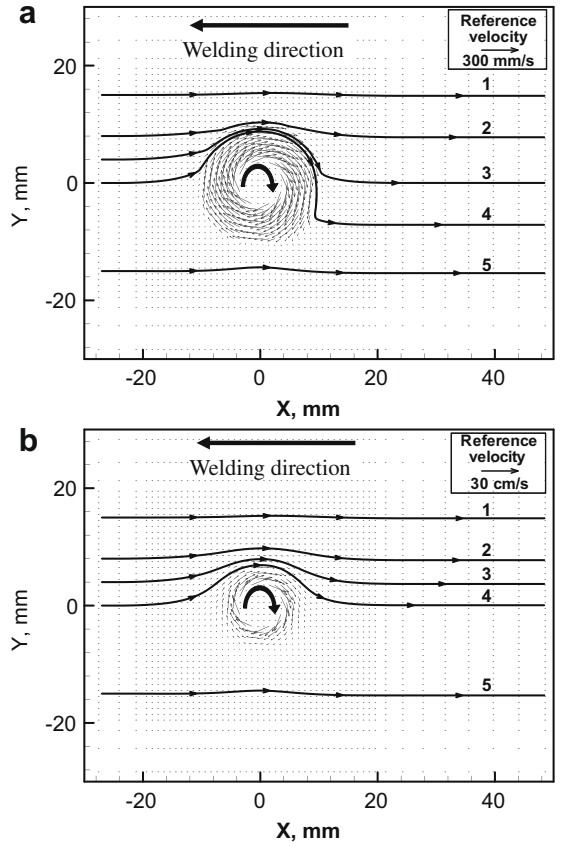

Figure 2. Velocity profile and streamlines used for calculation of strain values in (a) plane 1 and (b) plane 2. The tool shoulder and pin radii were 10.15 and 3.55 mm, respectively. FSW was done at 2.11 mm s^{-1} welding velocity, 300 rpm rotation speed and 42.3 kN axial force in a 300 mm × 210 mm × 6.4 mm workpiece.

width of the work piece with weld interface located at $y = 0$.

The velocity gradients along the five streamlines in Figure 2a are used to compute the strain rate components ($\dot{\varepsilon}_{ij}$), and the computed strain rates are integrated to determine the values of strain components (ε_{ij}) from Eq. (2). The computed values of two normal strain rate components $\dot{\varepsilon}_{11}$ and $\dot{\varepsilon}_{22}$ corresponding to the five streamlines are shown in Figure 3a and b, respectively. Considering the streamlines that pass through the retreating side, e.g., streamlines 1–4, in Figure 2a, the x-component of velocity, u, initially increases and then decreases with distance x as the material moves from the front to the back of the welding tool. Thus, the velocity gradient $\partial u/\partial x$, i.e., the strain rate component, $\dot{\varepsilon}_{11}$, is positive in front of the tool in Figure 3a. The velocity gradient becomes negative once the material crosses the tool. Consequently, $\dot{\varepsilon}_{11}$ is negative behind the welding tool for all the streamlines in Figure 3a. The y-component of velocity, v, initially decreases with increase in y in front of the tool and then decreases behind the tool as y decreases. Thus, the velocity gradient $\partial v/\partial y$, i.e., the strain rate component, $\dot{\varepsilon}_{22}$, is negative in front of the welding tool but becomes positive behind the tool (Fig. 3b).

As the rotating tool moves with the welding velocity, the material in the front is sheared and forced to accelerate through the retreating side in the direction opposite to the welding velocity. Thus, the longitudinal velocity of the material increases in the x-direction near the tool and then subsequently decreases as the material reaches behind the tool where the joint forms. The transverse velocity cannot increase appreciably due to proximity of the undeformed solid region within the work piece that remains unaffected by the rotational and translation movement of the tool.

The computed values of two normal strain components, ε_{11} and ε_{22}, are depicted in Figure 3c and d, respectively. As shown in Eq. (4), the calculation of strain components is cumulative in nature. Thus, the values of the strain components at any point on a streamline represent the cumulative effect of all the deformations the particle experienced before. The normal strain component ε_{11} increases as a particle moves along the streamline (Fig. 3c), indicating elongation of material along the x-direction up to the tool. As the strain rate becomes negative behind the welding tool, ε_{xx} decreases towards the end of the streamline, indicating that the material experiences compression along the

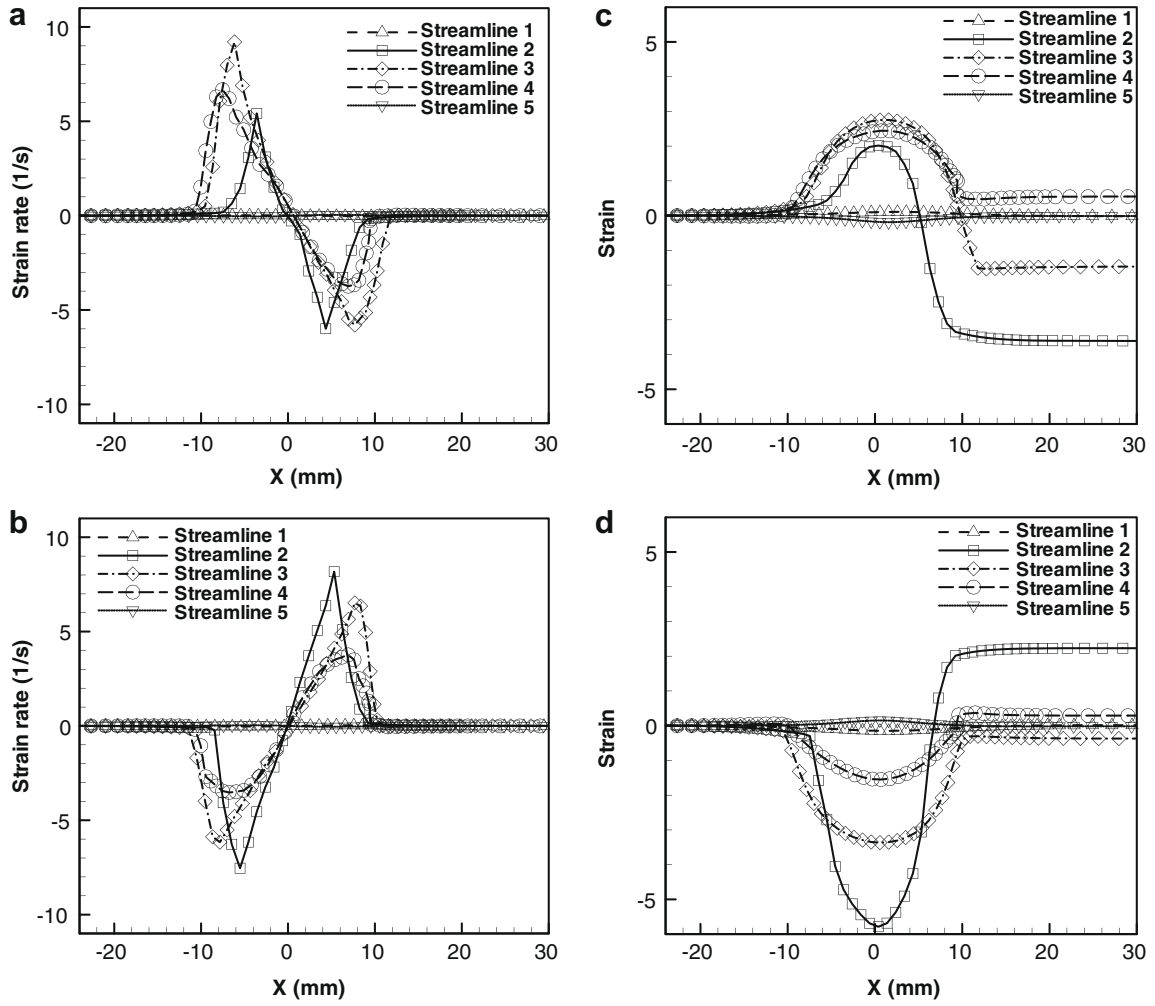

Figure 3. Computed strain rate components (a) $\dot{\varepsilon}_{11}$ and (b) $\dot{\varepsilon}_{22}$. Computed strain components (c) ε_{11} and (d) ε_{22}. FSW was done at 2.11 mm s^{-1} welding velocity, 300 rpm rotation speed and 42.3 kN axial force in a 300 mm × 210 mm × 6.4 mm workpiece. The tool shoulder and pin radii were 10.15 and 3.55 mm, respectively.

x-direction in these locations. In case of streamlines 2 and 3, ε_{11} becomes compressive towards the end of the streamline. However, in the case of streamline 4, ε_{11} retains a very small positive value (tensile strain) towards the end.

The transverse strain component, ε_{22}, shown in Figure 3d, decreases initially and then increases along the streamlines. Thus, ε_{22} is compressive in front of the welding tool. The addition of tensile strain component behind the welding tool reduces the magnitude of the compressive strain. Towards the end of the streamlines, ε_{22} is tensile in nature for material corresponding to the streamlines 2 and 4. However, for the material following streamline 3, ε_{22} is compressive in nature even towards the end with a very small magnitude.

The computed values of the local accumulated normal strain components around the moving tool are realistic in nature. For example, as the material in the front of the tool is transported through the retreating side, the material adjacent to the tool tends to elongate in the longitudinal direction and, therefore, compress in the transverse direction. Thus, the longitudinal strain, ε_{11}, is tensile (positive) and the transverse strain, ε_{22}, is compressive (negative) in the material in front of the tool. However, behind the tool, the longitudinal strain is compressive and the transverse strain is slightly tensile.

Figure 3c and d also show that the total in-plane strain, i.e., the sum of the two normal strain components ε_{11} (longitudinal) and ε_{22} (transverse) at any point along the streamlines 1 and 5, is very small. The sum of these strain components along the streamlines 2 and 3 is negative, while along the streamline 4 it is slightly positive. Since the summation of all three normal strain components at any point would be zero for zero dilation, the normal strain (ε_{33}) experienced by material will be negligible along streamlines 1 and 5, positive along streamlines 2 and 3, and negative along streamline 4. This trend fits well with the fact that streamlines 3 and 4 define approximately the boundary of the tool shoulder, with the former just outside and the latter just inside the shoulder periphery. Hence, the material along streamline 4, i.e., just within the edge of the shoulder periphery, will experience a compressive normal strain, while materials along streamlines 2 and 3 just outside the shoulder periphery will be subjected to bulging and hence experience tensile normal strains as also reported by Bastier et al. [11]. The strain rate and the strain components were also computed for planes further away from the work piece top surface. The absolute values of the strain and strain rate components were found to be smaller as distance from the tool shoulder in the thickness direction increases.

For the welding conditions investigated, the computed values of components of strain rate lies between -9 and $9\ s^{-1}$, whereas the computed values of strain components are between -10 to 5. These computed values of strain and strain rates are comparable to the earlier reported values for strain and strain rates [3,19].

The strain rate and strain components during FSW of AA2524 can be computed using a coupled three-dimensional viscoplastic flow and heat transfer model. As the material moves from the leading to the trailing edge through the retreating side, it experiences a tensile strain in the welding direction and compressive strain in the transverse direction. The nature of the strain reverses as the material reaches the trailing edge and is forced to consolidate behind the advancing tool. In the retreating side, the volumetric strain increases as the material reaches close to the tool and decreases behind the tool. The maximum strain occurs close to the welding tool. In the advancing side, the volumetric strains are small. For the condition of FSW investigated, the computed strains and strain rates were in the ranges -10 to 5 and -9 to $9\ s^{-1}$, respectively.

This research was supported by a grant from the Materials Division, Office of Naval Research, Johnnie DeLoach, Program Manager.

[1] M.D. Fuller, S. Swaminathan, A.P. Zhilyaev, T.R. McNelley, Materials Science and Engineering A 463 (2007) 128–137.
[2] F.J. Humphreys, P.B. Prangnell, J.R. Bowen, A. Gholinia, C. Harris, Philosophical Transactions of the Royal Society A 357 (1999) 1663–1681.
[3] T.R. McNelley, S. Swaminathan, J.Q. Su, Scripta Materialia 58 (2008) 349–354.
[4] P.B. Prangnell, C.P. Heason, Acta Materialia 53 (2005) 3179–3192.
[5] L.E. Murr, G. Liu, J.C. McClure, Journal of Materials Science Letters 16 (1997) 1801–1803.
[6] K. Oh-Ishi, A.P. Zhilyaev, T.R. McNelley, Metallurgical and Materials Transactions A 37A (2006) 277–286.
[7] J.Q. Sua, T.W. Nelson, C.J. Sterling, Materials Science and Engineering A 405 (2005) 277–286.
[8] G. Buffa, J. Hua, R. Shivpuri, L. Fratini, Materials Science and Engineering A 419 (2006) 381–388.
[9] G. Buffa, J. Hua, R. Shivpuri, L. Fratini, Materials Science and Engineering A 419 (2006) 389–396.
[10] H. Schmidt, J. Hattel, Modelling and Simulation in Materials Science and Engineering 13 (2005) 77–93.
[11] A. Bastier, M.H. Maitournam, K. Dang Van, F. Roger, Science and Technology of Welding and Joining 11 (3) (2006) 278–288.
[12] R. Nandan, T. DebRoy, H.K.D.H. Bhadeshia, Progress in Materials Science (2008) 980–1023.
[13] R. Nandan, G.G. Roy, T. DebRoy, Metallurgical and Materials Transactions A 37 (4) (2006) 1247–1259.
[14] R. Nandan, G.G. Roy, T.J. Lienert, T. DebRoy, Science and Technology of Welding and Joining 11 (5) (2006) 526–537.
[15] R. Nandan, G.G. Roy, T.J. Lienert, T. DebRoy, Acta Materialia 55 (2007) 883–895.
[16] R. Nandan, T.J. Lienert, T. DebRoy, International Journal of Materials Research 99 (4) (2008) 434–444.
[17] A. Arora, R. Nandan, A.P. Reynolds, T. DebRoy, Scripta Materialia 60 (2009) 13–16.
[18] D.G. Berghaus, H.B. Peacock, Experimental Mechanics 25 (3) (1985) 301–307.
[19] P. Heurtier, C. Desrayaud, F. Montheillet, Materials Science Forum 396–402 (2002) 1537–1542.